

# Magic wavelengths in the alkaline earth ions

Jasmeet Kaur<sup>a</sup>, Sukhjit Singh<sup>a</sup>, Bindiya Arora<sup>a\*</sup> and B. K. Sahoo<sup>b†</sup>

<sup>a</sup>*Department of Physics, Guru Nanak Dev University, Amritsar, Punjab-143005, India and*

<sup>b</sup>*Theoretical Physics Division, Physical Research Laboratory, Navrangpura, Ahmedabad-380009, India*

(Dated: Received date; Accepted date)

We present magic wavelengths for the  $nS - nP_{1/2,3/2}$  and  $nS - mD_{3/2,5/2}$  transitions, with the respective ground and first excited  $D$  states principal quantum numbers  $n$  and  $m$ , in the  $Mg^+$ ,  $Ca^+$ ,  $Sr^+$  and  $Ba^+$  alkaline earth ions for linearly polarized lights by plotting dynamic polarizabilities of the  $nS$ ,  $nP_{1/2,3/2}$  and  $mD_{3/2,5/2}$  states of the ions. These dynamic polarizabilities are evaluated by employing a relativistic all-order perturbative method and their accuracies are ratified by comparing their static values with the available high precision experimental or other theoretical results. Moreover, some of the magic wavelengths identified by us in  $Ca^+$  concurs with the recent measurements reported in [Phys. Rev. Lett. 114, 223001 (2015)]. Knowledge of these magic wavelengths are propitious to carry out many proposed high precision measurements trapping the above ions in the electric fields with the corresponding frequencies.

PACS numbers: 32.10 Dk, 31.15.Dv, 31.15.ap

State-insensitive trapping techniques have lead to tremendous advancements in the manipulation and control of atoms in far detuned optical traps. In this approach, the atoms are trapped at the wavelengths (related to frequencies) of an external electric field at which the differential light shift of an atomic transition, that is intended to be probed, due to the Stark effects nullify. These wavelengths are specially referred to as magic wavelengths ( $\lambda_{\text{magicS}}$ )[1]. It has been demonstrated earlier ability of trapping neutral atoms inside high- $Q$  cavities at  $\lambda_{\text{magicS}}$  in the strong coupling regime, which is important in the quantum computation and communication schemes [2]. This technique is now widely used to carry out many high precision measurements by eliminating large systematics due to stray electric fields. Another notable application of these wavelengths is to perform clock frequency measurements [3], especially for optical frequency standards [4], that are in turn useful to probe temporal and spatial variations of the fundamental constants [5] and improving global positioning systems [6]. Knowing  $\lambda_{\text{magicS}}$  of atomic systems are also very useful in the field of quantum state engineering [7], extracting out precise values of the oscillator strengths [8], etc. because of which extensive studies, both experimentally and theoretically, have been carried out in many atoms recently [6, 9–12]. On the other hand, singly charged alkaline earth ions are advantageous to carry out very high precision measurements using ion trapping and laser cooling techniques. Some of the prominent examples are the optical frequency standards [13, 14], probing variation of fundamental constants [3, 5], parity non-conservation effects [15, 16] etc. Advantages of these ions owe to their metastable  $D$  states that provide longer probe times during interrogation of measurements. To reduce system-

atics in these measurements, state insensitive measurements can be more pertinent that will require knowledge of  $\lambda_{\text{magicS}}$  in these ions. In fact,  $\lambda_{\text{magicS}}$  for the  $4S \rightarrow 3D_{3/2,5/2}$  and  $4S \rightarrow 4P_{1/2,3/2}$  transitions in  $Ca^+$  are recently observed [17].

In this Rapid Communication, we report  $\lambda_{\text{magicS}}$  for the  $nS - nP_{1/2,3/2}$  and  $nS - mD_{3/2,5/2}$  transitions in the  $Mg^+$ ,  $Ca^+$ ,  $Sr^+$  and  $Ba^+$  ions, for the principal quantum numbers of the ground state  $n$  and of the first excited  $D$  states  $m$  of the respective ions, for the commonly used linearly polarized lights in the experiments by evaluating dynamic dipole polarizabilities of these ions accurately.

Dominant contribution to the change in energy of a state  $|j_n, m_n\rangle$  with angular momentum  $j_n$  and its component  $m_n$  of an atomic system due to interaction with an external electric field  $\mathcal{E}(\omega)$  of frequency  $\omega$  is given by

$$\Delta E_{\text{Stark}} \approx -\frac{1}{2}\alpha_n(\omega)\mathcal{E}^2(\omega), \quad (1)$$

where  $\alpha_n(\omega)$  is the dynamic dipole polarizability of the atomic state  $|j_n, m_n\rangle$  and given by

$$\alpha_n(\omega) = \alpha_n^{(0)}(\omega) + \frac{3m_j^2 - j_n(j_n + 1)}{j_n(2j_n - 1)}\alpha_n^{(2)}(\omega), \quad (2)$$

for the scalar and tensor components as  $\alpha_n^{(0)}(\omega)$  and  $\alpha_n^{(2)}(\omega)$ , respectively. Expressions for these quantities in terms of the reduced electric dipole (E1) matrix elements can be found in Refs. [9–11]. As discussed in our previous work [18], we estimate  $\alpha_n^{(k)}$ s (for  $k = 0, 2$ ) by expressing

$$\alpha_n^{(k)} = \alpha_n^{(k)}(c) + \alpha_n^{(k)}(vc) + \alpha_n^{(k)}(v) \quad (3)$$

with the notations  $c$ ,  $vc$  and  $v$  representing the contributions due to the core, core-valence and valence correlation effects, respectively. Dominant valence correlations are estimated by calculating electric dipole (E1) matrix elements between many low-lying intermediate states and referred to as “Main” result. This is evaluated using

\*Email: arorabindiya@gmail.com

†Email: bijaya@prl.res.in

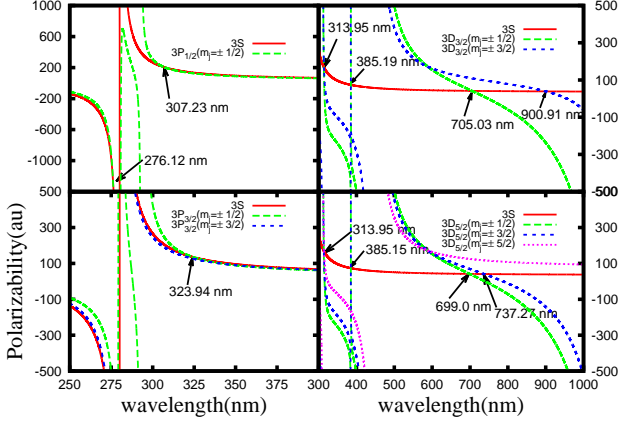


FIG. 1: (Color online) Dynamic polarizabilities (in au) of the  $3S_{1/2}$ ,  $3P_{1/2,3/2}$  and  $3D_{3/2,5/2}$  states in  $Mg^+$ . Arrows indicate positions of magic wavelengths ( $\lambda_{\text{magic}}$ ) in nm.

an all order relativistic coupled-cluster method with the singles and doubles approximation (SD method) as described in [19, 20]. Other small contributions from the higher excited states (referred to as “Tail” contribution), core and core-valence correlations are estimated using lower order perturbative methods as described in [18]. To construct the single particle orbitals for the SD method, we have used total 70 B-spline functions with a cavity of radius  $R = 220$  au. However, a few E1 matrix elements involving the  $F_{5/2,7/2}$  states in  $Ba^+$  are taken from [21] to use as many as E1 matrix elements for more accurate evaluations of the Main contributions to  $\alpha_n$ s of the  $5D$  states of this ion. Estimated static polarizabilities in the above procedure of the considered ground and excited states of the alkaline earth metal ions using these matrix elements and experimental energies from national institute of standards and technology (NIST) [22] are listed in the Supplemental material along with the individual core, core-valence and Tail contributions. These values are also compared with the available precise experimental results and theoretical calculations. We find excellent agreement between our results with these values implying that our calculations are precise enough to predict the magic wavelengths in the considered ions reliably.

In Tables I, II, III and IV, we list  $\lambda_{\text{magic}}$ s for the  $nS - nP_{1/2,3/2}$  and  $nS - mD_{3/2,5/2}$  transitions in the  $Mg^+$ ,  $Ca^+$ ,  $Sr^+$  and  $Ba^+$  ions respectively. They are obtained by locating the crossings between the dynamic polarizabilities of the  $nS$ ,  $nP_{1/2}$ ,  $nP_{3/2}$ ,  $mD_{3/2}$ , and  $mD_{5/2}$  states of  $Mg^+$ ,  $Ca^+$ ,  $Sr^+$  and  $Ba^+$  plotted against the frequencies as shown in Figs. 1, 2, 3 and 4 respectively. The arrows in the figures indicate the positions of  $\lambda_{\text{magic}}(\text{avg})$  values which are the average of the magic wavelengths at different  $m_j$  sub-levels. The  $\lambda_{\text{magic}}(\text{avg})$  are not presented for cases where magic wavelengths are (a) not identified for all  $m_j$  sub-levels, (b) supporting different kind of traps for all  $m_j$  sublevels (c) separated by large

TABLE I: Magic wavelengths ( $\lambda_{\text{magic}}$ s) in nm and corresponding polarizabilities (in au) in the  $Mg^+$  ion. List of the resonant wavelengths ( $\lambda_{\text{res}}$ s) and  $\lambda_{\text{magic}}$ s are also given sequentially in increasing order to indicate their respective placements.

Resonance	$\lambda_{\text{res}}$	$ m_j $	$\lambda_{\text{magic}}$	$\alpha(\lambda_{\text{magic}})$
<hr/>				
Transition			$3S - 3P_{1/2}$	
$3P_{1/2} - 3D_{3/2}$	279.0777	1/2	276.12	-1267.54
$3P_{1/2} - 3S_{1/2}$	280.2704			
$3P_{1/2} - 4S_{1/2}$	292.8683	1/2	307.23	202.59
<hr/>				
Transition			$3S - 3P_{3/2}$	
$3P_{3/2} - 3D_{3/2}$	279.7930			
$3P_{3/2} - 3D_{5/2}$	279.7998			
$3P_{3/2} - 3S_{1/2}$	279.5528			
$3P_{3/2} - 4S_{1/2}$	293.6510	1/2	323.94	136.51
<hr/>				
Transition			$3S - 3D_{3/2}$	
$3D_{3/2} - 5F_{5/2}$	310.4809	1/2	313.73	169.42
		3/2	314.18	167.53
$3D_{3/2} - 5P_{3/2}$	384.8335	3/2	385.01	72.56
$3D_{3/2} - 5P_{1/2}$	385.0385	1/2	385.38	73.47
$3D_{3/2} - 4F_{5/2}$	448.1327	1/2	705.03	41.44
		3/2	900.91	38.67
<hr/>				
$3D_{3/2} - 4P_{3/2}$	1091.5270			
$3D_{3/2} - 4P_{1/2}$	1095.1779			
<hr/>				
Transition			$3S - 3D_{5/2}$	
$3D_{5/2} - 5F_{7/2}$	310.4715			
$3D_{5/2} - 5F_{5/2}$	310.4721	1/2	313.67	169.66
		3/2	313.80	169.01
		5/2	314.39	166.70
$3D_{5/2} - 5P_{3/2}$	384.8209	3/2	385.12	73.58
		1/2	385.17	73.56
<hr/>				
$3D_{5/2} - 4F_{7/2}$	448.1130			
$3D_{5/2} - 4F_{5/2}$	448.1150	1/2	699.0	41.57
		3/2	737.27	40.79
$3D_{5/2} - 4P_{3/2}$	1091.423			
<hr/>				

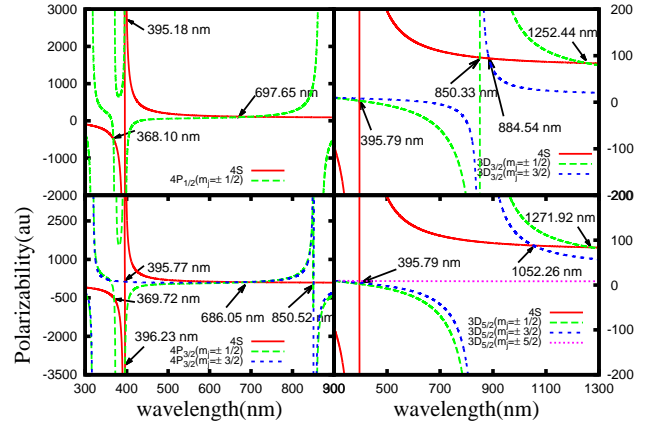


FIG. 2: (Color online) Dynamic polarizabilities (in au) of the  $4S_{1/2}$ ,  $4P_{1/2,3/2}$  and  $3D_{3/2,5/2}$  states in  $Ca^+$ . Locations of average  $\lambda_{\text{magic}}$ s (in nm) are indicated by arrows.

wavelengths for different  $m_j$  sub-levels. We also give the total  $\alpha_n$  values at the corresponding  $\lambda_{\text{magic}}$ s considering different  $m_j$  values in the tables. Before we proceed in

TABLE II:  $\lambda_{\text{magic}}$ s (in nm) and corresponding polarizabilities (in au) in the  $\text{Ca}^+$  ion.  $\lambda_{\text{res}}$  are also presented to identify the placements of  $\lambda_{\text{magic}}$ s clearly between two resonant wavelengths. Results from this work ([T]) are compared with the findings from Ref. [8].

Resonances Transition	$\lambda_{\text{res}}$	$ m_j $	$\lambda_{\text{magic}}$	$\alpha(\lambda_{\text{magic}})$	Reference
<u><math>4S - 4P_{1/2}</math></u>					
$4P_{1/2} - 4D_{3/2}$	315.887	1/2	368.10	-485.18	[T]
			368.0149	-477.2554	[8]
$4P_{1/2} - 5S_{1/2}$	370.603	1/2	395.18	2933.47	[T]
			395.1807	2896.7954	[8]
$4P_{1/2} - 4S_{1/2}$	396.847	1/2	697.65	110.39	[T]
			690.817	110.0849	[8]
$4P_{1/2} - 3D_{3/2}$	866.214				
<u><math>4S - 4P_{3/2}</math></u>					
$4P_{3/2} - 4D_{5/2}$	317.933				
$4P_{3/2} - 4D_{3/2}$	318.128	1/2	369.72	-520.85	[T]
			369.6393	-512.1655	[8]
$4P_{3/2} - 5S_{1/2}$	373.690				
$4P_{3/2} - 4S_{1/2}$	393.366	3/2	395.77	125.27	[T]
			395.774	123.4906	[8]
		1/2	396.23	-3118.47	[T]
			396.2315	-3077.3881	[8]
$4S_{1/2} - 4P_{1/2}$	396.847	3/2	678.35	113.38	[T]
			672.508	113.0150	[8]
		1/2	693.76	110.96	[T]
			687.022	110.6606	[8]
$4P_{3/2} - 3D_{3/2}$	849.802	1/2	850.12	81.57	[T]
		3/2	850.92	96.09	[T]
$4P_{3/2} - 3D_{5/2}$	854.209				
<u><math>4S - 3D_{3/2}</math></u>					
$4S_{1/2} - 4P_{3/2}$	393.366	1/2	395.80	3.13	[T]
			395.7981	1.1711	[8]
		3/2	395.79	8.02	[T]
			395.7970	7.1019	[8]
$4S_{1/2} - 4P_{1/2}$	396.847				
$3D_{3/2} - 4P_{3/2}$	849.802	1/2	850.33	96.12	[T]
			850.335	95.0011	[8]
$3D_{3/2} - 4P_{1/2}$	866.214	3/2	884.54	94.23	[T]
			887.382	92.9908	[8]
		1/2	1252.44	84.17	[T]
			1308.590	82.4644	[8]
<u><math>4S - 3D_{5/2}</math></u>					
$4S_{1/2} - 4P_{3/2}$	393.366	1/2	395.79	2.44	[T]
			395.7982	0.5371	[8]
		3/2	395.79	3.49	[T]
			395.7978	3.1792	[8]
		5/2	395.79	8.83	[T]
			395.7968	8.4633	[8]
$4S_{1/2} - 4P_{1/2}$	396.847				
$3D_{5/2} - 4P_{3/2}$	854.209	3/2	1052.26	88.06	[T]
			1074.336	86.4837	[8]
		1/2	1271.92	83.90	[T]
			1338.474	82.1167	[8]

presenting  $\lambda_{\text{magic}}$ s, we would like to clarify that  $\alpha_n$ s of the  $nS$  states can have two important resonant transitions ( $nS - nP_{1/2}$  and  $nS - nP_{3/2}$ ) in the wavelength range

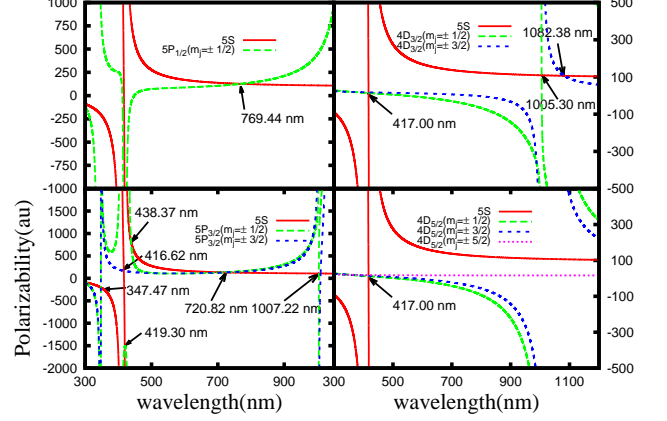


FIG. 3: (Color online) Dynamic polarizabilities (in au) of the  $5S_{1/2}$ ,  $5P_{1/2,3/2}$  and  $4D_{3/2,5/2}$  states in  $\text{Sr}^+$ . Arrows indicate positions of the average  $\lambda_{\text{magic}}$  in nm.

considered in this work. Therefore,  $\alpha_n$ s of the  $nS$  states are generally small except in the close vicinity of these transitions. In contrast,  $\alpha_n$ s of the  $nP$  and  $mD$  states can have significant contributions from several resonant transitions in the considered wavelength range. Thus, they are expected to cross with  $\alpha_n$ s of the  $nS$  states between these resonant transitions. We also list the resonant wavelengths ( $\lambda_{\text{res}}$ ) in the above tables to highlight respective placements of  $\lambda_{\text{magic}}$ s. We find similar trends in locating magic wavelengths for all the considered ions, except for few cases where  $\lambda_{\text{magic}}$ s are missing.

**Mg<sup>+</sup>:** We are able to locate two  $\lambda_{\text{magic}}$ s magic wavelengths for the  $3S - 3P_{1/2}$  transition in  $\text{Mg}^+$ , one just before the  $3P_{1/2} - 3D$  resonant transition at 276.12 nm and one just after the  $3P_{1/2} - 4S$  resonant transition at 307.23 nm. The first  $\lambda_{\text{magic}}$  supports a blue detuned trap, whereas the second one a red detuned trap. However, only one  $\lambda_{\text{magic}}$  for the  $3S - 3P_{3/2}(m_j = \pm 1/2)$  transition is located at 323.94 nm and nothing is found for the  $3S - 3P_{3/2}(m_j = \pm 3/2)$  transition. On the other hand, three  $\lambda_{\text{magic}}$ s are identified for the  $3D_{3/2} - 3S$  transition placed between six different resonances. First one is located around 314 nm between the  $3D_{3/2} - 5F_{5/2}$  and  $3D_{3/2} - 5P_{3/2}$  resonant transitions. The next  $\lambda_{\text{magic}}$  is located at the sharp intersection of polarizability curves close to the  $3D_{3/2} - 5P_{3/2}$  and the  $3D_{3/2} - 5P_{1/2}$  resonances as seen in Fig. 1. The last  $\lambda_{\text{magic}}$  is located at 705.03 nm for  $m_j = \pm 1/2$  and 900.91 nm for  $m_j = \pm 3/2$  sub-levels, hence it is of limited experimental use. For the  $3S - 3D_{5/2}$  transition, only one  $\lambda_{\text{magic}}$  appears for all  $m_j$  sub-levels around 314 nm. All the observed  $\lambda_{\text{magic}}$ s along with the  $\lambda_{\text{res}}$ s are tabulated in Table I. It can be noticed from this table that most of these magic wavelengths favor weak red detuned traps.

**Ca<sup>+</sup>:** At least three  $\lambda_{\text{magic}}$ s are located for the  $4P_{1/2} - 4S$  transition in  $\text{Ca}^+$  at 368.10, 395.18 and 697.65 nms between the  $4P_{1/2} - 4D_{3/2}$ ,  $4P_{1/2} - 5S$ ,  $4P_{1/2} - 4S$  and

TABLE III:  $\lambda_{\text{magic}}$ s (in nm) and their corresponding polarizabilities (in au) in  $\text{Sr}^+$  and  $\lambda_{\text{res}}$  contributing to the polarizabilities of the transitional states are also listed.

Resonances	$\lambda_{\text{res}}$	$ m_j $	$\lambda_{\text{magic}}$	$\alpha(\lambda_{\text{magic}})$
Transition $5S - 5P_{1/2}$				
$5P_{1/2} - 5D_{3/2}$	338.0711			
$5P_{1/2} - 6S_{1/2}$	416.1796			
$5P_{1/2} - 5S_{1/2}$	421.5524	1/2	769.44	126.34
$5P_{1/2} - 4D_{3/2}$	1091.4874			
Transition $5S - 5P_{3/2}$				
$5P_{3/2} - 5D_{5/2}$	346.4457	3/2	347.38	-204.86
$5P_{3/2} - 5D_{3/2}$	347.4887	1/2	347.57	-205.66
$5P_{3/2} - 5S_{1/2}$	407.7714	3/2	416.62	168.54
		1/2	419.30	-1521.68
$5S_{1/2} - 5P_{1/2}$	421.5524			
$5P_{3/2} - 6S_{1/2}$	430.5447	1/2	438.37	817.75
		1/2	716.72	134.25
		3/2	724.92	132.83
$5P_{3/2} - 4D_{3/2}$	1003.6654	1/2	1004.47	108.08
		3/2	1009.80	108.90
Transition $5S - 4D_{3/2}$				
$5S_{1/2} - 5P_{3/2}$	407.7714	3/2	417.00	17.36
		1/2	417.00	13.83
$5S_{1/2} - 5P_{1/2}$	421.5524			
$4D_{3/2} - 5P_{3/2}$	1003.6654	1/2	1005.30	108.93
		3/2	1082.38	106.29
Transition $5S - 4D_{5/2}$				
$5S_{1/2} - 5P_{3/2}$	407.7714	1/2	417.01	12.16
		5/2	417.00	18.43
		3/2	417.00	14.25
$5S_{1/2} - 5P_{1/2}$	421.5524			
$4D_{5/2} - 5P_{3/2}$	1032.7309			

TABLE IV:  $\lambda_{\text{magic}}$ s (in nm) and their corresponding polarizabilities (in au) in  $\text{Ba}^+$ .  $\lambda_{\text{res}}$ s are also given to identify the placements of  $\lambda_{\text{magic}}$ s between them.

Resonances	$\lambda_{\text{res}}$	$ m_j $	$\lambda_{\text{magic}}$	$\alpha(\lambda_{\text{magic}})$
Transition $6S - 6P_{1/2}$				
$6P_{1/2} - 8S_{1/2}$	264.72608	1/2	323.33	-93.74
$6P_{1/2} - 6D_{3/2}$	389.17790	1/2	451.73	-4574.49
$6P_{1/2} - 7S_{1/2}$	452.4926	1/2	468.90	953.80
$6P_{1/2} - 6S_{1/2}$	493.4077	1/2	599.28	311.58
$6P_{1/2} - 5D_{3/2}$	649.6898			
Transition $6S - 6P_{3/2}$				
$6P_{3/2} - 8S_{1/2}$	277.13528	3/2	348.85	-133.47
		1/2	360.63	-158.70
$6P_{3/2} - 6D_{5/2}$	413.06491			
$6P_{3/2} - 6D_{3/2}$	416.60014	1/2	416.66	-460.38
		3/2	416.06	-459.32
$6P_{3/2} - 6S_{1/2}$	455.4033	3/2	475.72	374.67
$6P_{3/2} - 7S_{1/2}$	489.9927	1/2	552.60	441.01
		3/2	561.01	406.42
$6S_{1/2} - 6P_{1/2}$	493.4077			
$6P_{3/2} - 5D_{3/2}$	585.3675	1/2	586.24	336.10
		3/2	593.40	321.95
Transition $6S - 5D_{3/2}$				
$6S_{1/2} - 6P_{3/2}$	455.4033	3/2	480.44	15.88
		1/2	480.81	-15.82
$6S_{1/2} - 6P_{1/2}$	493.4077			
$5D_{3/2} - 6P_{3/2}$	585.3675	1/2	585.98	336.18
		3/2	592.46	323.72
$5D_{3/2} - 6P_{1/2}$	649.6898	1/2	767.81	194.05
Transition $6S - 5D_{5/2}$				
$6S_{1/2} - 6P_{3/2}$	455.4033	5/2	480.26	31.04
		3/2	480.71	-7.19
		1/2	480.93	-26.46
$6S_{1/2} - 6P_{1/2}$	493.4077			
$5D_{5/2} - 6P_{3/2}$	614.1713	3/2	666.64	239.13
		1/2	718.18	211.13

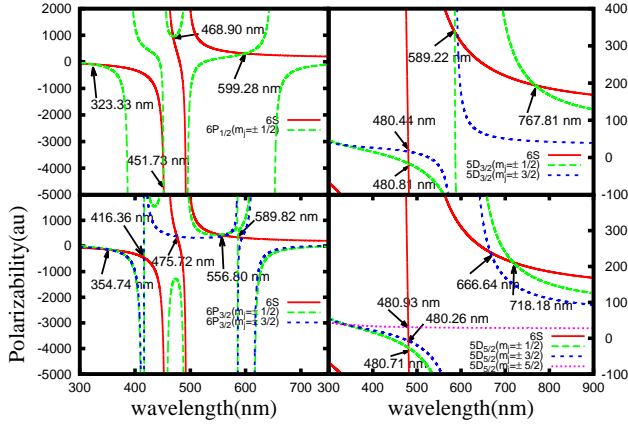


FIG. 4: (Color online) Dynamic polarizabilities (in au) of the  $6S_{1/2}$ ,  $6P_{1/2,3/2}$  and  $5D_{3/2,5/2}$  states in  $\text{Ba}^+$  with their average  $\lambda_{\text{magic}}$ s (in nm) pointed by arrows.

$4P_{1/2} - 3D_{3/2}$  resonant transitions. A good agreement is found between our results and findings by Tang et al. [8] except for our  $\lambda_{\text{magic}}$  at 697.65 nm, which is red

detuned as compared to their value. Similarly, a total of four  $\lambda_{\text{magic}}$ s are located for the  $4S - 4P_{3/2}$  transition as shown in Fig. 2 and listed in Table II. We also find  $\lambda_{\text{magic}}$ s at 395.77 nm and 396.23 nm for the  $4S - 4P_{3/2}$  transition within the fine structure splittings of the  $4P$  states which coincides with the experimental observations at 395.7992(7) nm and 395.7990(7) nm respectively [17]. Similar to the  $4P_{1/2} - 4S$  transition, the other observed  $\lambda_{\text{magic}}$ s at 678.35 nm and 693.76 nm are red detuned as compared to findings in Ref. [8]. Moreover, they have missed a  $\lambda_{\text{magic}}$  around 850 nm which lies in between the  $4P_{3/2} - 3D_{3/2}$  and  $4P_{3/2} - 3D_{5/2}$  resonant transitions.  $\lambda_{\text{magic}}$ s for the  $4S - 3D_{3/2}$  and  $4S - 3D_{5/2}$  transitions, detected between the fine structure splitting of the  $4P$  state at 395.79 nm, offer a scope to trap  $\text{Ca}^+$  at very small polarizabilities and are not much of practical use. As seen in Fig. 2,  $\alpha_n$ s of the  $3D_{5/2}(m_j = \pm 5/2)$  state attain a constant value throughout the wavelength range considered in this work. Consequently, only one crossing is noticed for this state at 395 nm when  $\alpha_n$  of the  $4S$  state changes

sign close to the  $4S - 4P$  resonances. The other identified  $\lambda_{\text{magic}}$ s at 1052.26, 1252.44 and 1271.92 nms for the  $4S - 3D_{3/2}$  and  $4S - 3D_{5/2}$  transitions with different  $m_j$  values are blue detuned compared to the earlier findings of Ref. [8]. The possible reasons for these disagreements could be that the plots for  $\alpha_n$ s of the transitional states cross at very small angles at these wavelengths thus making them very in-distinctive. Moreover, Tang *et. al.* have performed semi-empirical calculations of polarizabilities in the relativistic framework that do not take into account electron correlation effects rigorously like our SD method.

**Sr<sup>+</sup>:** From Fig. 3, we are able to locate only one magic wavelength at 769.44 nm for the  $5S - 5P_{1/2}$  transition of Sr<sup>+</sup>. As given in Table III,  $\lambda_{\text{magic}}$ s for the  $5S - 5P_{3/2}$  transition are, however, systematically placed between various resonances. We also locate a crossing between the  $5S$  and  $5P_{3/2}(m_j = \pm 1/2)$  states at 438.37 nm. All identified  $\lambda_{\text{magic}}$ s for the  $5S - 5P_{3/2}$  transition are typically small in magnitude with exception for  $\lambda_{\text{magic}} = 419.302$  nm. At this  $\lambda_{\text{magic}}$ , it is recommended to use blue tuned trap for the  $m_j = \pm 1/2$  sub-levels of Sr<sup>+</sup>. For the  $4D_{3/2} \rightarrow 5S$  transition,  $\lambda_{\text{magic}} = 1007.22$  nm lies in the infrared region and is recommended for red detuned trap. In Fig. 3, we also observe that  $\alpha_n$ s for the transitional states at  $\lambda_{\text{magic}} = 417$  nm for the  $5S - 4D_{3/2}$  and  $5S - 4D_{5/2}$  transitions are very small (almost approach to zero). Therefore, it may not be advantageous to trap the Sr<sup>+</sup> ion at this wavelength.

**Ba<sup>+</sup>:** Four  $\lambda_{\text{magic}}$ s are found for the  $6S - 6P_{1/2}$  tran-

sition in Ba<sup>+</sup> at 323.33, 451.73, 468.90 and 599.28 nms among which  $\lambda_{\text{magic}} = 451.73$  nm is in direct vicinity of the  $6P_{1/2} - 7S_{1/2}$  resonance (within 0.8 nm) yielding a very large negative value of  $\alpha_n$ . However, the other  $\lambda_{\text{magic}}$ s are at far distances from the photon excitation energies of the resonant transitions yielding small  $\alpha_n$ s. We also identify at least five  $\lambda_{\text{magic}}$ s for the  $6P_{3/2} - 6S_{1/2}$  transition placed systematically between various resonant transitions. Similarly, several  $\lambda_{\text{magic}}$ s are also located for the  $6S - 5D_{3/2}$  and  $6S - 5D_{5/2}$  transitions as seen in Fig. 4 in the wavelength range 300-800 nm and listed in Table IV.

*Conclusion:* By determining dynamic dipole polarizabilities of the ground  $nS$  and the first excited  $nP_{1/2,3/2}$  and  $mD_{3/2,5/2}$  states, many magic wavelengths of the  $nS - nP_{1/2,3/2}$  and  $nS - mD_{3/2,5/2}$  transitions of the Mg<sup>+</sup>, Ca<sup>+</sup>, Sr<sup>+</sup> and Ba<sup>+</sup> alkaline earth metal ions are identified. Occurrence of magic wavelengths are predicted between the resonant wavelengths which will be very helpful to perform high precision measurements in the above ions using both the red and blue tuned trapping techniques.

*Acknowledgement:* The work is supported by CSIR Grant No. 03(1268)/13/EMR-II, India, and UGC-BSR Grant No. F.7-273/2009/BSR. A part of the computations were carried out using Vikram-100 HPC cluster of Physical Research Laboratory and the employed SD method was developed in the group of Professor M. S. Safronova of Delaware University, USA.

- 
- [1] H. Katori, T. Ido, and M. K. Gonokami, J. Phys. Soc. Jpn. **68**, 2479 (1999).
- [2] J. McKeever, J. R. Buck, A. D. Boozer, A. Kuzmich, H.-C. Nagerl, D. M. Stamper-Kurn, and H. J. Kimble, Phys. Rev. Lett. **90**, 133602 (2003).
- [3] H. S. Margolis, J. Phys. B **42**, 154017 (2009).
- [4] V. D. Ovsiannikov and V. G. Palchikov, Laser Physics **15**, 1040 (2005).
- [5] S. G. Karshenboim and E. Peik, *Astrophysics, Clocks and Fundamental Constants*, 3-540-21967-6 (Springer, Springer Verlag Berlin Heidelberg, 2004).
- [6] T. Hong, C. Cramer, E. Cook, W. Nagourney, and E. N. Fortson, Opt. Lett. **30**, 2644 (2005).
- [7] C. A. Sackett, D. Kielpinski, B. E. King, C. Langer, V. Meyer, C. J. Myatt, M. Rowe, Q. A. Turchette, W. M. Itano, D. J. Wineland, et al., Nature **404**, 256 (2000).
- [8] Y. B. Tang, H. X. Qiao, T. Y. Shi, and J. Mitroy, Phys. Rev. A **87**, 042517 (2013).
- [9] B. Arora, M. S. Safronova, and C. W. Clark, Phys. Rev. A **76**, 052509 (2007).
- [10] B. Arora and B. K. Sahoo, Phys. Rev. A **86**, 033416 (2012).
- [11] B. K. Sahoo and B. Arora, Phys. Rev. A **87**, 023402 (2013).
- [12] M. Takamoto, F.-L. Hong, R. Higashi, and H. Katori, Nature (London) **435**, 321 (2005).
- [13] M. Kajita, Y. Li, K. Matsubara, K. Hayasaka, and M. Hosokawa, Phys. Rev. A **72**, 043404 (2005).
- [14] P. Dubé, A. A. Madej, J. Bernard, L. Marmet, J. S. Boulanger, and S. Cundy, Appl. Phys. Lett. **95**, 033001 (2005).
- [15] N. Fortson, Phys. Rev. Lett. **70**, 2383 (1993).
- [16] B. K. Sahoo, P. Mandal, and M. Mukherjee, Phys. Rev. A **83**, 030502(R) (2011).
- [17] P. Liu, Y. Huang, W. Bian, H. Shao, H. Guan, Y. Tang, C. Li, J. Mitroy, and K. Gao, Phys. Rev. Lett. **114**, 223001 (2015).
- [18] J. Kaur, D. K. Nandy, B. Arora, and B. Sahoo, Phys. Rev. A **91**, 012705 (2015).
- [19] S. A. Blundell, W. R. Johnson, and J. Sapirstein, Phys. Rev. A **43**, 3407 (1991).
- [20] M. S. Safronova, A. Derevianko, and W. R. Johnson, Phys. Rev. A **58**, 1016 (1998).
- [21] B. K. Sahoo, L. W. Wansbeck, K. Jungmann, and R. G. E. Timmermans, Phys. Rev. A **79**, 052512 (2009).
- [22] A. Kramida, Y. Ralchenko, J. Reader, and N. A. T. (2012), *Nist atomic spectra database* (2012), (version 5). [Online]. Available: <http://physics.nist.gov/asd> [2012, December 12]. National Institute of Standards and Technology, Gaithersburg, MD.

## Supplemental Material

In a sum-over-states approach the valence correlation contributions can be estimated using the expression

$$\alpha_n^{(0)}(v) = -\frac{2}{3(2j_n+1)} \sum_{p \neq n} \frac{(E_p - E_n) |\langle j_n || D || j_p \rangle|^2}{(E_n - E_p)^2 - \omega^2} \quad (1)$$

and

$$\begin{aligned} \alpha_n^{(2)}(v) = & -8 \sum_{p \neq n} (-1)^{j_n+j_p+1} \begin{Bmatrix} j_n & 1 & j_n \\ 1 & j_p & 2 \end{Bmatrix} \\ & \times \sqrt{\frac{5j_n(2j_n-1)}{6(j_n+1)(2j_n+1)(2j_n+3)}} \\ & \times \frac{(E_p - E_n) |\langle j_n || D || j_p \rangle|^2}{(E_n - E_p)^2 - \omega^2}, \end{aligned} \quad (2)$$

where  $p$  stands for the excited intermediate states,  $j_s$  are angular momentum of the correspond state,  $E_s$  are their energies and  $D$  is the dipole operator. It is required to calculate a sufficient number of atomic states so that as many as E1 matrix elements  $\langle j_n || D || j_p \rangle$  can be evaluated to estimate contributions to the  $\alpha_n^{(k)}$  values. Contributions from the higher excited states, especially from the continuum, are usually small and they can be estimated using a lower order many-body method to a reasonable accuracy as suggested in our previous work [1]. We refer the above described dominant contribution as ‘‘Main’’ and the later contribution as ‘‘Tail’’ to  $\alpha_n^{(k)}(v)$ .

Similarly, the core-valence contribution can be estimated by expressing as

$$\alpha_n^{(0)}(cv) = -\frac{2}{3(2j_n+1)} \sum_c \frac{(E_c - E_n) |\langle j_n || D || j_c \rangle|^2}{(E_n - E_c)^2 - \omega^2} \quad (3)$$

and

$$\begin{aligned} \alpha_n^{(2)}(cv) = & -8 \sum_c (-1)^{j_n+j_c+1} \begin{Bmatrix} j_n & 1 & j_n \\ 1 & j_c & 2 \end{Bmatrix} \\ & \times \sqrt{\frac{5j_n(2j_n-1)}{6(j_n+1)(2j_n+1)(2j_n+3)}} \\ & \times \frac{(E_c - E_n) |\langle j_n || D || j_c \rangle|^2}{(E_n - E_c)^2 - \omega^2}, \end{aligned} \quad (4)$$

where  $c$  stands for core orbitals. This basically subtracts the extra contributions accounted by allowing the Pauli’s exclusion principle of the valence electron in the determination of the atomic states. Typically, these contributions are extremely small in magnitude and can be estimated using a lower order many-body theory as in Ref. [1].

Expressions for the core contributions is given by

$$\alpha_n^{(0)}(c) = -\frac{2}{3} \sum_{c,p} \frac{(E_c - E_p) |\langle j_p || D || j_c \rangle|^2}{(E_p - E_c)^2 - \omega^2}. \quad (5)$$

and

$$\begin{aligned} \alpha_n^{(2)}(c) = & -8 \sum_{c,p} (-1)^{j_p+j_c+1} \begin{Bmatrix} j_p & 1 & j_p \\ 1 & j_c & 2 \end{Bmatrix} \\ & \times \sqrt{\frac{5j_n(2j_n-1)(2j_n+1)}{6(j_n+1)(2j_n+3)}} \\ & \times \frac{(E_c - E_p) |\langle j_p || D || j_c \rangle|^2}{(E_p - E_c)^2 - \omega^2}, \end{aligned} \quad (6)$$

where  $c$  and  $p$  represent sums over core and virtual orbitals, respectively. It can be noticed that there appears an extra phase factor in the expression for the tensor polarizability. Since  $c$  and  $p$  sums over a complete set of  $c$  and  $p$  orbitals of a closed-core, therefore core contribution to the tensor polarizability nullifies. Again, the core contributions to the scalar polarizabilities for the states having common core are same since its expression is independent of  $j_n$ .

The first four low-lying allowed transitions are included in the evaluations of the ‘‘Main’’ contributions in the  $\text{Mg}^+$ ,  $\text{Ca}^+$  and  $\text{Sr}^+$  ions, whereas only the first three low-lying allowed transitions are included in the  $\text{Ba}^+$  ion. However, the first six low-lying E1 matrix elements are included in the estimation of ‘‘Main’’ contributions in the  $3D_{3/2,5/2}$  states of the  $\text{Ca}^+$  ion. These states are evaluated using a linearized version of the relativistic coupled-cluster method with the singles and doubles approximation (SD method) as described in Refs. [2, 3]. Atomic wave function of the  $|j_n, m_n\rangle$  state in this method is given by

$$\begin{aligned} |\Psi_n\rangle = & \left[ 1 + \sum_{pa} \rho_{pa} a_p^\dagger a_a + \frac{1}{2} \sum_{pqab} \rho_{pqab} a_p^\dagger a_q^\dagger a_b a_a \right. \\ & \left. + \sum_{p \neq n} \rho_{pn} a_p^\dagger a_n + \sum_{pqa} a_p^\dagger a_q^\dagger a_a a_n \right] |\Phi_n\rangle, \end{aligned} \quad (7)$$

where  $|\Phi_n\rangle$  is considered to be the Dirac-Fock (DF) wave function constructed by

$$|\Phi_n\rangle = a_n^\dagger |\Phi_0\rangle \quad (8)$$

for the DF wave function  $|\Phi_0\rangle$  of the closed-core. In the above expression,  $a_i^\dagger$  and  $a_i$  represent for the creation and annihilation operators. The indices  $p, q$  represent for the virtual orbitals and the indices  $a, b$  refer to the occupied orbitals.  $\rho_s$  are the amplitudes of the excitations with the subscripts for the corresponding orbitals. The matrix element of  $D$  between states  $|j_v m_v\rangle$  and  $|j_w m_w\rangle$  states is evaluated in this method by [4].

$$D_{vw} = \frac{\langle \psi_v || D || \Psi_w \rangle}{\sqrt{\langle \psi_v | \psi_v \rangle \langle \psi_w | \psi_w \rangle}}. \quad (9)$$

Combining E1 matrix elements obtained using the SD method with the experimental energies from the national

TABLE I: Calculated values of the static dipole polarizabilities of  $\text{Ca}^+$ ,  $\text{Sr}^+$ ,  $\text{Ba}^+$  and  $\text{Ra}^+$  alkaline earth metal ions. These values are compared with the other available theoretical and experimental results. References are given in the square brackets. The first four low-lying allowed transitions were included in the evaluations of the “Main” contributions in the  $\text{Mg}^+$ ,  $\text{Ca}^+$  and  $\text{Sr}^+$  ions, whereas only the first three low-lying allowed transitions were included in the  $\text{Ba}^+$  ion. In an exception, the first six low-lying E1 matrix elements were included in the estimation of “Main” contributions in the  $3D_{3/2,5/2}$  states of the  $\text{Ca}^+$  ion.

$\text{Mg}^+$	$\alpha^{(0)}(3S_{1/2})$	$\alpha^{(0)}(3P_{1/2})$	$\alpha^{(0)}(3P_{3/2})$	$\alpha^{(2)}(3P_{3/2})$	$\alpha^{(0)}(3D_{3/2})$	$\alpha^{(2)}(3D_{3/2})$	$\alpha^{(0)}(3D_{5/2})$	$\alpha^{(2)}(3D_{5/2})$
Main	34.50	30.89	31.18	1.32	185.35	-78.41	184.71	-111.13
Core	0.48	0.48	0.48	-	0.48	-	0.48	-
Core-valence	$-1.32 \times 10^{-2}$	0.0	0.0	-	$-1.12 \times 10^{-3}$	-	$-1.70 \times 10^{-3}$	-
Tail	$6.66 \times 10^{-2}$	0.23	0.23	-0.16	3.46	-0.73	3.46	-1.04
Total (Present)	35.04	31.60	31.88	1.157	189.29	-79.137	188.65	-112.18
Others [6]	35.01	31.598	31.598	1.163	188.6	-112.1	188.6	-112.1
Experiment [7]	35.02(4)	-	-	-	-	-	-	-
$\text{Ca}^+$	$\alpha^{(0)}(4S_{1/2})$	$\alpha^{(0)}(4P_{1/2})$	$\alpha^{(0)}(4P_{3/2})$	$\alpha^{(2)}(4P_{3/2})$	$\alpha^{(0)}(3D_{3/2})$	$\alpha^{(2)}(3D_{3/2})$	$\alpha^{(0)}(3D_{5/2})$	$\alpha^{(2)}(3D_{5/2})$
Main	72.80	-4.97	-2.96	10.74	26.23	-16.45	25.98	-23.11
Core	3.26	3.26	3.26	-	3.26	-	3.26	-
Core-valence	$-8.85 \times 10^{-2}$	0.0	0.0	-	$-7.94 \times 10^{-3}$	-	$-1.20 \times 10^{-2}$	-
Tail	$5.87 \times 10^{-2}$	2.52	2.52	-0.66	3.05	-0.62	2.84	-0.82
Total (Present)	76.03	0.82	2.82	10.08	32.31	-17.02	32.05	-23.92
Others [8]	75.28	-2.774	-0.931	10.12	32.99	-17.88	32.81	-25.16
Others [9]	76.1(5)	-0.75(70)	1.02(64)	10.31(28)	32.0(3)	-17.43(23)	31.8(3)	-24.51(29)
Experiment [10]	75.3(4)	-	-	-	-	-	-	-
$\text{Sr}^+$	$\alpha^{(0)}(5S_{1/2})$	$\alpha^{(0)}(5P_{1/2})$	$\alpha^{(0)}(5P_{3/2})$	$\alpha^{(2)}(5P_{3/2})$	$\alpha^{(0)}(4D_{3/2})$	$\alpha^{(2)}(4D_{3/2})$	$\alpha^{(0)}(4D_{5/2})$	$\alpha^{(2)}(4D_{5/2})$
Main	85.73	-39.94	-28.44	11.33	53.83	-34.25	53.63	-46.33
Core	4.98	4.98	4.98	-	4.98	-	4.98	-
Core-valence	-0.19	0.0	0.0	-	$-1.77 \times 10^{-2}$	-	$-2.79 \times 10^{-2}$	-
Tail	$1.97 \times 10^{-2}$	3.70	2.67	-0.81	4.95	-1.00	3.48	-1.01
Total(Present)	90.54	-31.27	-20.79	10.52	63.74	-35.26	62.08	-47.35
Other [11]	89.88	-23.13	-23.13	-	61.77	-	61.77	-
Other [12]	88.29(1.0)	-	-	-	61.43(52)	-35.42(25)	62.87(75)	-48.83(30)
Experiment [13]	93.3(9)	-32.6	-32.6	-	57.0	-	57.0	-
$\text{Ba}^+$	$\alpha^{(0)}(6S_{1/2})$	$\alpha^{(0)}(6P_{1/2})$	$\alpha^{(0)}(6P_{3/2})$	$\alpha^{(2)}(6P_{3/2})$	$\alpha^{(0)}(5D_{3/2})$	$\alpha^{(2)}(5D_{3/2})$	$\alpha^{(0)}(5D_{5/2})$	$\alpha^{(2)}(5D_{5/2})$
Main	114.19	6.85	32.00	5.87	39.71	-21.92	42.42	-30.37
Core	9.35	9.35	9.35	-	9.35	-	9.35	-
Core-valence	-0.38	0.0	0.0	-	$-2.35 \times 10^{-2}$	-	$-3.87 \times 10^{-2}$	-
Tail	$1.66 \times 10^{-2}$	4.26	4.18	-1.17	4.76	-1.00	4.80	-1.47
Total (Present)	123.18	20.46	45.53	4.70	53.80	-22.92	56.53	-31.83
Other [12]	124.26(1.0)	-	-	-	48.81(46)	-24.62(28)	50.67(58)	-30.85(31)
Experiment [14]	123.88(5)	-	-	-	-	-	-	-

institute of standards and technology (NIST) database [5], we determine the “Main” contributions to valence correlations of  $\alpha_n$ s of the  $nS_{1/2}$ ,  $nP_{1/2,3/2}$  and  $mD_{3/2,5/2}$  states in the considered alkaline earth metal ions. In Table I, we list the contributions from the “Main”, core, valence-core and “Tail” components to the static values of  $\alpha_n$  for all the considered alkaline ions. The final values are compared with other available theoretical and experimental values. Transitions up to the  $3S - 6P$ ,  $3P - 6S$ ,  $3P - 6d$ ,  $3D - 6P$  and  $3D - 7F$  are included into the “Main” contribution for  $\text{Mg}^+$  ion. As seen from

Table I, the ground state dipole polarizability values obtained for the  $\text{Mg}^+$  ion are very close to the values estimated by Mitroy and Zhang [6]. They evaluate the non-relativistic values of polarizabilities by diagonalizing the semi-empirical Hamiltonian in a large dimension single electron basis. We notice that there is a large difference between our polarizability results for  $3D_{3/2}$  and  $3D_{5/2}$  states and hence the non-relativistic values calculated by them are unfavorable. Snow [7] deduced the static polarizability for the ground state of the  $\text{Mg}^+$  ion from the fine structure of high Rydberg levels. Their  $\alpha^{(0)}$  value

of  $35.02(0.04) a_0^3$  agrees well with our result of  $35.04 a_0^3$ . For  $\text{Ca}^+$  ion transitions up to the  $4S - 7P$ ,  $4P - 7S$ ,  $4P - 6d$ ,  $3D - 7P$  and  $3D - 7F$  are included into the "Main" contribution. While examining polarizabilities in case of the  $\text{Ca}^+$  ion, we notice that our calculation for the ground state polarizability is in the agreement with the result obtained from experimental spectral analysis by Chang [10]. Also, a comparison of our calculated polarizabilities for this ion with the calculations done using combination of many-body perturbation theory and SD scaled method by Safronova *et al.* [9] shows very good agreement. Moreover, our result for the ground state is in consistent agreement with the results calculated by Tang and co-workers [8]. However, a discrepancy has been observed between our results and other calculations among the  $P$  state polarizabilities this ion. We notice that the polarizabilities of the  $P$  states are very small due to substantial cancellations between some large contributions to the total polarizability. The final values are, thus, very sensitive to these cancellations. Next, we compare our polarizability results for the  $\text{Sr}^+$  ion in Table I. Transitions up to the  $5S - 8P$ ,  $5P - 8S$ ,  $5P - 7d$ ,  $4D - 8P$  and  $3D - 7F$  are included into the "Main" contribution for this ion. Mitroy and coworkers [11] have used a non-relativistic method using a sum-over-states approach to determine polarizabilities of the  $S$ ,  $P$  and  $D$  states of  $\text{Sr}^+$ .

It is evident from Table I that our ground state dipole polarizability is in agreement with their result. However, it may not be proper to compare their non-relativistic values of the polarizabilities for the  $4D_{3/2}$  and  $4D_{5/2}$  states just by including corrections from the relativistic effects with the non-relativistic values against our fully relativistic calculations. However, the static dipole polarizabilities calculated for the ground and  $4D$  state of the  $\text{Sr}^+$  ion using an *ab initio* relativistic coupled-cluster method [12] are in close agreement with our results. There are no direct experimental values available to compare with these results. The polarizability values for the  $S$ ,  $P$  and  $D$  states of the  $\text{Sr}^+$  ion, derived by combining the experimental results with oscillator strength sums by Barklem and O'Mara [13], has a considerable discrepancy with our present results. In  $\text{Ba}^+$  ion, transitions up to the  $6S - 8P$ ,  $6P - 8S$ ,  $6P - 6d$ ,  $5D - 8P$  and  $5D - 7F$  are included into the "Main" contribution. The high-precision ground state polarizability measurement for  $\text{Ba}^+$ , achieved by using a novel technique, based on the resonant excitation Stark ionization spectroscopy [14], is in very good agreement with our work. To summarize, the above analysis clearly justifies that our calculations of dipole polarizabilities in the considered alkaline earth metal ions are accurate enough to predict the magic wavelengths in these ions reliably.

- 
- [1] J. Kaur, D. K. Nandy, B. Arora, and B. K. Sahoo, Phys. Rev A **91**, 012705 (2015).
- [2] S. A. Blundell, W. R. Johnson, and J. Sapirstein, Phys. Rev A **43**, 3407 (1991).
- [3] M. S. Safronova, A. Derevianko, and W. R. Johnson, Phys. Rev A **58**, 1016 (1998).
- [4] M. S. Safronova, *Ph.D. Thesis* (University of Notre Dame, 2000).
- [5] A. Kramida, Y. Ralchenko, J. Reader, and N. A. T. (2012), *Nist atomic spectra database* (2012), (version 5). [Online]. Available: <http://physics.nist.gov/asd> [2012, December 12]. National Institute of Standards and Technology, Gaithersburg, MD.
- [6] J. Mitroy and J. Y. Zhang, Eur. Phys. J. D. **46**, 415 (2008).
- [7] E. Snow, *Ph.D. Thesis* (Colorado State University, 2006).
- [8] Y. B. Tang, H. X. Qaio, T. Y. Shi, and J. Mitroy, Phys. Rev. A **87**, 042517 (2013).
- [9] M. S. Safronova and U. I. Safronova, Phys. Rev. A **83**, 012503 (2011).
- [10] E. S. Chang, J. Phys. B: At. Mol. Phys. **16**, L539 (1983).
- [11] J. Mitroy, J. Y. Zhang, and M. W. Bromley, Phys. Rev. A **77**, 032512 (2008).
- [12] B. K. Sahoo, R. G. E. Timmermans, B. P. Das, and D. Mukherjee, Phys. Rev A **80**, 062506 (2009).
- [13] P. S. Barklem and B. J. O'Mara, Mon. Not. R. Astron. Soc. **311**, 535 (2000).
- [14] E. L. Snow and S. R. Lundeen, Phys. Rev. A **76**, 052505 (2007).